

REVIEW



Imaging in acute respiratory distress syndrome

Antonio Pesenti^{1,2*} , Guido Musch³, Daniel Lichtenstein⁴, Francesco Mojoli^{5,6}, Marcelo B. P. Amato⁷, Gilda Cinnella⁸, Luciano Gattinoni⁹ and Michael Quintel⁹

© 2016 Springer-Verlag Berlin Heidelberg and ESICM

Abstract

Purpose: Imaging has become increasingly important across medical specialties for diagnostic, monitoring, and investigative purposes in acute respiratory distress syndrome (ARDS).

Methods: This review addresses the use of imaging techniques for the diagnosis and management of ARDS as well as gaining knowledge about its pathogenesis and pathophysiology. The techniques described in this article are computed tomography, positron emission tomography, and two easily accessible imaging techniques available at the bedside—ultrasound and electrical impedance tomography (EIT).

Results: The use of computed tomography has provided new insights into ARDS pathophysiology, demonstrating that ARDS does not homogeneously affect the lung parenchyma and that lung injury severity is widely distributed in the ARDS population. Positron emission tomography is a functional imaging technique whose value resides in adding incremental insights to morphological imaging. It can quantify regional perfusion, ventilation, aeration, lung vascular permeability, edema, and inflammation. Lung ultrasound and EIT are radiation-free, noninvasive tools available at the bedside. Lung ultrasound can provide useful information on ARDS diagnosis when x-rays or CT scan are not available. EIT is a useful tool to monitor lung ventilation and to assess the regional distribution of perfusion.

Conclusions: The future of imaging in critical care will probably develop in two main directions: easily accessible imaging techniques that can be used at the bedside and sophisticated imaging methods that will be used to aid in difficult diagnostic cases or to advance our understanding of the pathogenesis and pathophysiology of an array of critical illnesses.

Keywords: Computed tomography, Positron emission tomography, Lung ultrasound, Electrical impedance tomography, Acute respiratory distress syndrome

*Correspondence: antonio.pesenti@unimi.it

¹ Dipartimento di Anestesia, Rianimazione ed Emergenza Urgenza, Fondazione IRCCS Cà Granda-Ospedale Maggiore Policlinico, Via Francesco Sforza 35, 20122 Milan, Italy
Full author information is available at the end of the article

Take-home message: Chest imaging has been used in the diagnosis of acute respiratory distress syndrome (ARDS) since its first description in 1967. Computed tomography fundamentally changed the view of the pathology demonstrating that ARDS does not homogeneously affect the lung parenchyma. Positron emission tomography added functional information to the morphological data and suggested that at least a part of the normally aerated baby lung is inflamed. Lung ultrasound and electrical impedance tomography are radiation-free, noninvasive tools available at the bedside and useful for diagnosis and monitoring of ARDS patients.

Introduction

Acute respiratory distress syndrome (ARDS) was first introduced 50 years ago and multiple definitions have been proposed over time up to the recent Berlin definition. Limited information, however, is available about the epidemiology, recognition, management, and outcomes of patients. Recent findings indicate that ARDS represents 10.4 % of ICU admissions and that 60.2 % of all patients with ARDS are clinician-recognized, indicating the potential for improvement in the diagnosis and management [1]. In this context, imaging techniques may be useful tools. In fact, imaging in critical care has

become more and more important: some techniques such as ultrasound and electrical impedance tomography are used at the bedside, while other imaging methods are useful in difficult diagnostic cases or to advance our understanding of an array of critical illnesses. This review article addresses both these domains in relation to ARDS.

CT scan in ARDS

History

The use of computed tomography (CT) in ARDS was first reported by Rommelsheim in 1983 [2]. The paper described “dorso-central distribution of densities observed especially during the edematous phase of the syndrome”. Unfortunately, this report (in German) was ignored by the scientific community. Two later papers [3, 4], published independently in April 1986, changed our vision of ARDS. They showed that ARDS densities are not homogeneously diffused, as chest x-rays mostly suggested, but are mainly distributed in the dependent lung regions. Moreover, the study from Milan reported the CT scan effects of PEEP, showing dramatic decrease of densities in some patients and no change in others.

Quantitative CT scan analysis

The image produced by the CT scan consists of a matrix of pixels, each representing a volume element of the tissue (voxel). CT scan measures the attenuation coefficient (μ), i.e., the reduction of the radiation intensity upon passage through matter. A μ value is assigned to each voxel (μ_{voxel}), roughly proportional to its density, and is expressed as a CT number standardized to that of water (μ_{water}):

$$\text{CT} = 1000 \times \frac{\mu_{\text{voxel}} - \mu_{\text{water}}}{\mu_{\text{water}}}$$

As an example, a voxel whose CT number is -700 HU is composed of 30 % of tissue (assuming a tissue density of 1 g/cm^3) and 70 % of gas. From density we compute both the gas and the tissue volumes of a given region or of the whole lung, defining its state of aeration (from collapse to hyperinflation).

Since tissue density is assumed to be equal to that of water (i.e., 1 g/cm^3) then tissue volume equals tissue weight.

Lung compartments at different degrees of aeration, from totally non-aerated to hyperinflated tissue [5], can be defined by analyzing the CT number frequency distribution of all the voxels included in the lung profile.

The discriminant power of the CT scan is remarkable. Modern CT scanners may acquire the entire volume of the thorax in less than a breath hold, returning an imaged volume consisting of virtually cubic voxels with a volume

of $0.216\text{--}0.343 \text{ mm}^3$. The volume of a normal acinus, which includes approximately 2000 alveoli, is about $16\text{--}22 \text{ mm}^3$ at functional residual capacity (FRC). This implies that the voxel volume is nearly 1/100 of the acinus volume at FRC, i.e., the volume of approximately 20 alveoli.

The more traditional CT scan protocol introduced used one to three axial images to infer the whole lung behavior. This protocol, however, has been questioned because it is less representative of the whole lung and it is impossible to scan exactly the same anatomical structure as the lung “moves” in different settings [6]. The availability of faster CT scanners allows the continuous CT scanning of the entire lung but it is difficult to rescan the entire patient under multiple test conditions because of x-ray exposure. A good compromise has been found with the extrapolation from ten thoracic CT sections, a method that can reduce radiation exposure and shorten the time required for the analysis [7].

CT scan and lung mechanics

CT scan consistently showed that the decreased gas volume of the ARDS lung is primarily responsible for its mechanical characteristics and that the lung compliance is proportional to the residual ventilable lung [5]. The smaller the open lung is, the lower the compliance is. Therefore, the lung was small, rather than stiff, as originally described [8]. This observation led to the concept of “baby lung”, which contributed to explain the possible harm of the mechanical ventilation in ARDS. Over the years the “baby lung” concept evolved [9], but the main concept remains valid: a “normal” tidal volume delivered to small baby lungs in ARDS patients may induce greatly supraphysiological tissue strains and damage. Moreover, hyperinflation (defined as the presence of voxels with a density between -1000 and -900 HU) is present in severe ARDS patients characterized by large non-aerated compartments even at 6 mL/kg ventilation [10].

CT scan and recruitment

Airspace collapse during ARDS is primarily the result of increased superimposed pressure due to the presence of edema [11]. The assessment of the recruitability of the collapsed lung is relevant to select an appropriate level of PEEP. In fact, both physiological studies [12, 13] and meta-analysis on patients from large PEEP trials [14] suggested that the patients with severe ARDS may benefit from higher PEEP levels. Several approaches have been used to estimate the recruitment: improvement of gas exchange [15], changes of lung mechanics [16], ultrasound modifications [17], and electrical impedance variations [18]. It is worth noting that these methods, which measure different entities, are not

necessarily interchangeable. For recruitability assessment, two CT scans are taken at different airway pressures (5 and 45 cmH₂O) to measure the amount of non-aerated lung (+100 HU and -100 HU) regaining inflation at high pressure (potential for lung recruitment). With this method, Gattinoni et al. found that recruitability is largely variable in ARDS patients and that it increases with ARDS severity [13] (Fig. 1).

A second approach, although using the same terminology and HU thresholds of the voxel-by-voxel analysis, is based both on morphology and density analysis [6]. In a given lung region, well identified through anatomical markers, the contiguous voxels with inflation up to -500 HU (non-aerated or poorly aerated) are identified by a color code and manually contoured. The manual delineation performed on the CT section obtained at zero end-expiratory pressure (ZEEP) is translated to the CT scan performed at PEEP using anatomical landmarks such as pulmonary vessels or segmental bronchi and recruitment is computed as the difference of CT gas volume measured in the counter-lung regions. Obviously, the two methods give different results [19]. The voxel-by-voxel analysis measures the amount of tissue which will likely undergo intratidal collapse and decollapse, a variable monotonically related to mortality, while the anatomical method measures both the tissue regaining inflation and the tissue shifting from poorly aerated to a normally aerated status, without discriminating the two. In addition, the morphological approach led to definition of ARDS as lobar, patchy, and diffuse. It is tempting to speculate that lobar pneumonia is more frequent in mild ARDS, the patchy in intermediate ARDS, while the diffuse pneumonia is more frequent in severe ARDS. A definite relationship between morphology and function, however, is still lacking.

CT scan, stress, strain, and homogeneity

Strain is the deformation of lung tissue (tidal volume to FRC ratio) when a transpulmonary pressure is applied. The opposite reactive force rising in the tissue is called stress. The total lung strain can be estimated through the measurement of FRC by helium dilution or other techniques [20]. What makes the CT scan unique, however, is the regional measurement of lung strain. The strain difference between contiguous structures is the key measurement to estimate the lung homogeneity [21]. In a homogeneous material, an applied force should cause the same strain in each one of its part. In contrast, if the strain is different in different voxels, we may infer that the forces acting locally, and the resulting local stress, are also proportionally different. Cressoni et al. found, with the CT scan, that locally the stress may be near twofold

the applied pressure [21]. The amount of voxels in which this phenomenon may occur (called “stress risers”) increases with ARDS severity. Higher PEEP levels may decrease this phenomenon [21].

CT scan in clinical practice

In ARDS patients, a CT scan, even using lower x-ray exposure [22], taken possibly under standard conditions at PEEP 5 cmH₂O [23] will allow one to diagnose unexpected findings and may guide the choice of appropriate respiratory treatment. Even the visual inspection of a standard CT scan enables to assess the amount and the distribution of densities as well as to detect pleural effusions [24] or localized tension pneumothoraxes not detectable with the standard x-rays. The acquisition of a second CT scan at 45 cmH₂O airway pressure allows one to assess lung recruitability. Therefore, even the visual inspection provides robust insights into the amount of edema, and lung recruitability, which are the anatomical and physiological basis for PEEP selection. Quantitative CT scan analysis, however, allows one to measure the lung weight, the fractions of tissue open and closed to ventilation, how much tissue can be recruited, and to what extent the stress risers are distributed. This information might allow a rational use of PEEP values and prone position.

PET imaging of ARDS

Positron emission tomography (PET) has been increasingly used to study the pathophysiology of ARDS and ventilator-induced lung injury (VILI) both in clinical and experimental studies. PET is versatile and it can quantify regional perfusion, ventilation, aeration, lung vascular permeability, edema, metabolic activity of inflammatory cells, enzyme activity, and pulmonary gene expression [25].

PET imaging of regional lung function in ARDS and VILI

The tracers most frequently used are [¹⁵O]oxygen-labeled water (H₂¹⁵O) to measure regional perfusion and lung water; [¹³N]nitrogen (¹³N₂), either dissolved in saline solution and injected intravenously, to measure regional perfusion, shunt, ventilation of perfused alveoli and gas trapping, or administered by inhalation to measure regional aeration and ventilation (including dead-space ventilation); ¹¹C, in the form of carbon monoxide (¹¹CO), to derive extravascular lung water (EVLW) from H₂¹⁵O measurements of lung water, or as ¹¹C-methylalbumin to measure vascular permeability. ⁶⁸Ga-transferrin can also be used to measure permeability and ⁶⁸Ga-albumin aggregates have been used to measure the regional distribution of pulmonary perfusion in experimental studies [26].

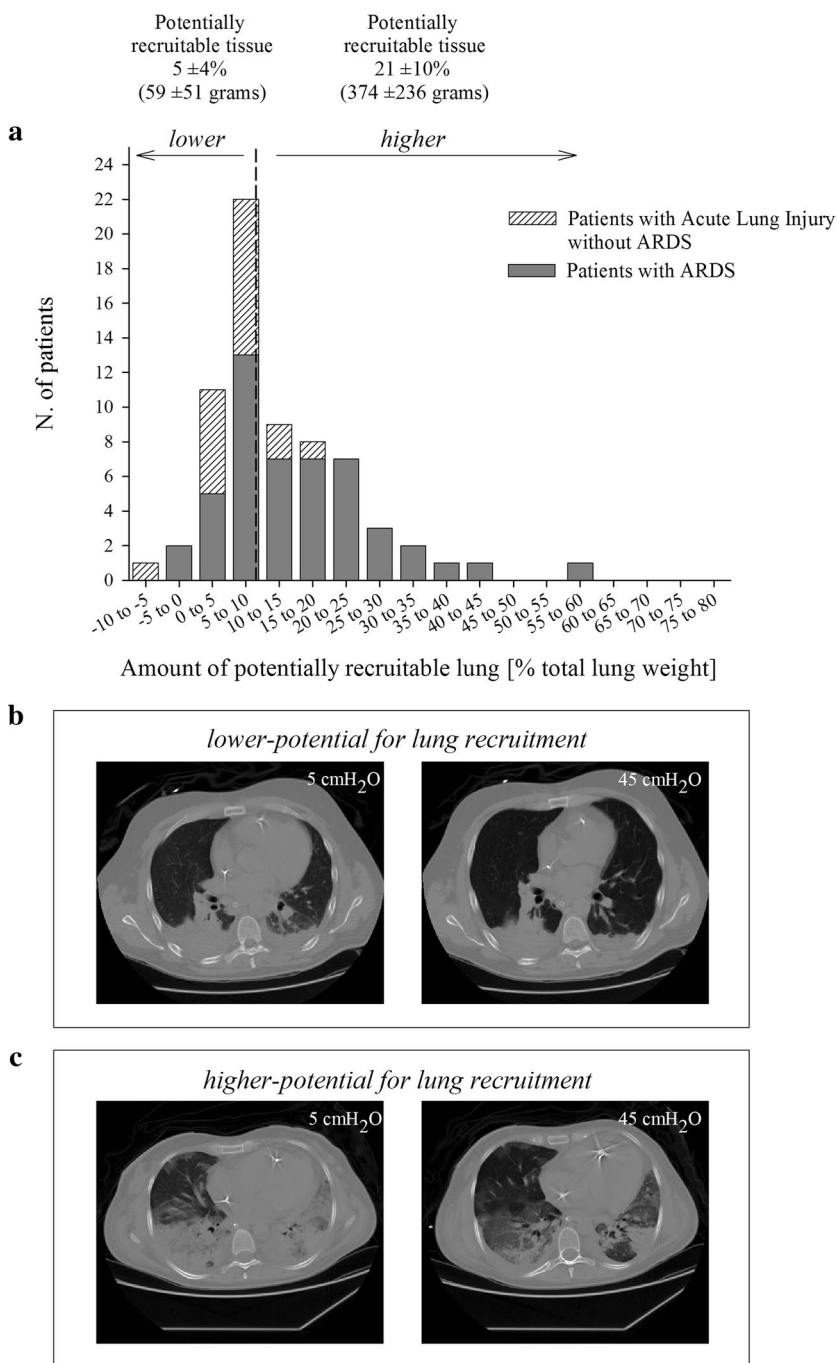


Fig. 1 **a** Frequency distribution of 68 ARDS patients according to the amount of lung recruitability, expressed as the percentage of the total lung weight. ALI without ARDS was defined by a $\text{PaO}_2/\text{FiO}_2$ of less than 300 but not less than 200, and ARDS was defined by a $\text{PaO}_2/\text{FiO}_2$ of less than 200. The amount of potentially recruitable lung was defined as the proportion of lung tissue in which aeration was restored at airway pressures between 5 and 45 cmH_2O . **b** Representative CT slices of the lung obtained 2 cm above the diaphragm dome at airway pressures of 5 cmH_2O (left) and 45 cmH_2O (right) from a patient with a lower percentage of potentially recruitable lung (at or below the median value of 9% of total lung weight). **c** Representative CT slices of the lung obtained 2 cm above the diaphragm dome at airway pressures of 5 cmH_2O (left) and 45 cmH_2O (right) from a patient in the group with a higher percentage of potentially recruitable lung (Reproduced from Gattinoni et al. [13])

The value of PET resides in the incremental insights it adds to morphological imaging. As an example, CT scan has shown that in patients with ARDS, normally aerated lung coexists with derecruited lung, predominant in dependent regions. However, PET has revealed that the increase in pulmonary vascular permeability is uniform throughout the ARDS lung, without a ventrodorsal gradient [27], indicating that even normally aerated regions are affected by the disease process. Furthermore, PET measurements of regional perfusion have shown an inverse relationship between the fraction of pulmonary blood flow to dependent lung regions and the subject's $\text{PaO}_2/\text{FiO}_2$ ratio [28]. This implies that subjects with the same amount and distribution of lung opacities (i.e., with the same clinical CT or chest x-ray picture) can have markedly different PaO_2 , and hence "clinical severity" of ARDS, depending on how efficiently their perfusion redistributes away from non-aerated regions. Combined PET measurements of perfusion and shunt have also identified redistribution of perfusion toward derecruited regions as the mechanism for the worsening of oxygenation sometimes observed with recruitment maneuvers [29] or PEEP [30]. Taken together, these findings indicate that the clinician must be cautious when using PaO_2 as an index of ARDS severity or of response to recruitment strategies if the distribution of perfusion is unknown.

The possibility to perform serial PET scans has allowed insights into the temporal evolution of disease processes associated with ARDS. Experimental studies using PET with ^{68}Ga -albumin aggregates have shown a biphasic response to acid aspiration, a frequent cause of ARDS. Within 10 min and for the first hour after aspiration, blood flow to affected regions increases, suggesting a hyperemic response triggered by the initial insult. However, by as early as 2 h, perfusion is lower in regions with aspiration than in spared regions [31], likely as a result of hypoxic pulmonary vasoconstriction or direct vascular compression by the exudate.

PET imaging of inflammatory cell activity

Activated inflammatory cells, particularly neutrophils, rely heavily on anaerobic glycolysis. PET with 2- ^{18}F fluoro-2-deoxy-D-glucose (^{18}F FDG) has been used to measure regional neutrophil metabolic activation in lung inflammation [32, 33] and VILI [34]. Since the original case report of increased pulmonary ^{18}F FDG uptake in ARDS [35], subsequent studies have confirmed that the metabolic activity of the ARDS lung is increased compared with normal controls [25]. Such an increase involves not only consolidated CT scan areas but also parenchyma with normal density (Fig. 3 of Ref. [9]). In fact, whereas in some patients the highest ^{18}F FDG uptake occurs in areas with the highest density, in others it occurs within aerated, normal density lung regions

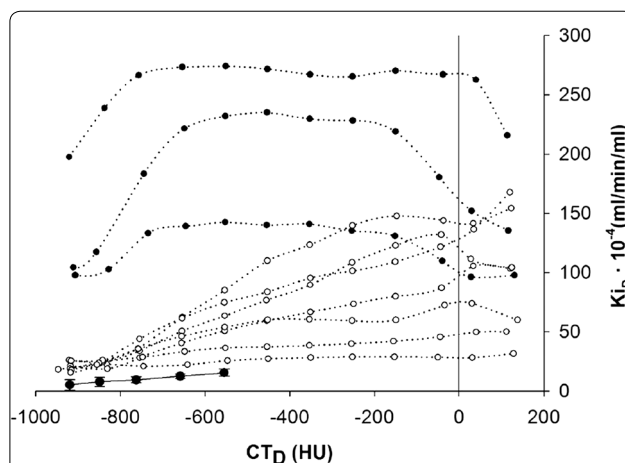
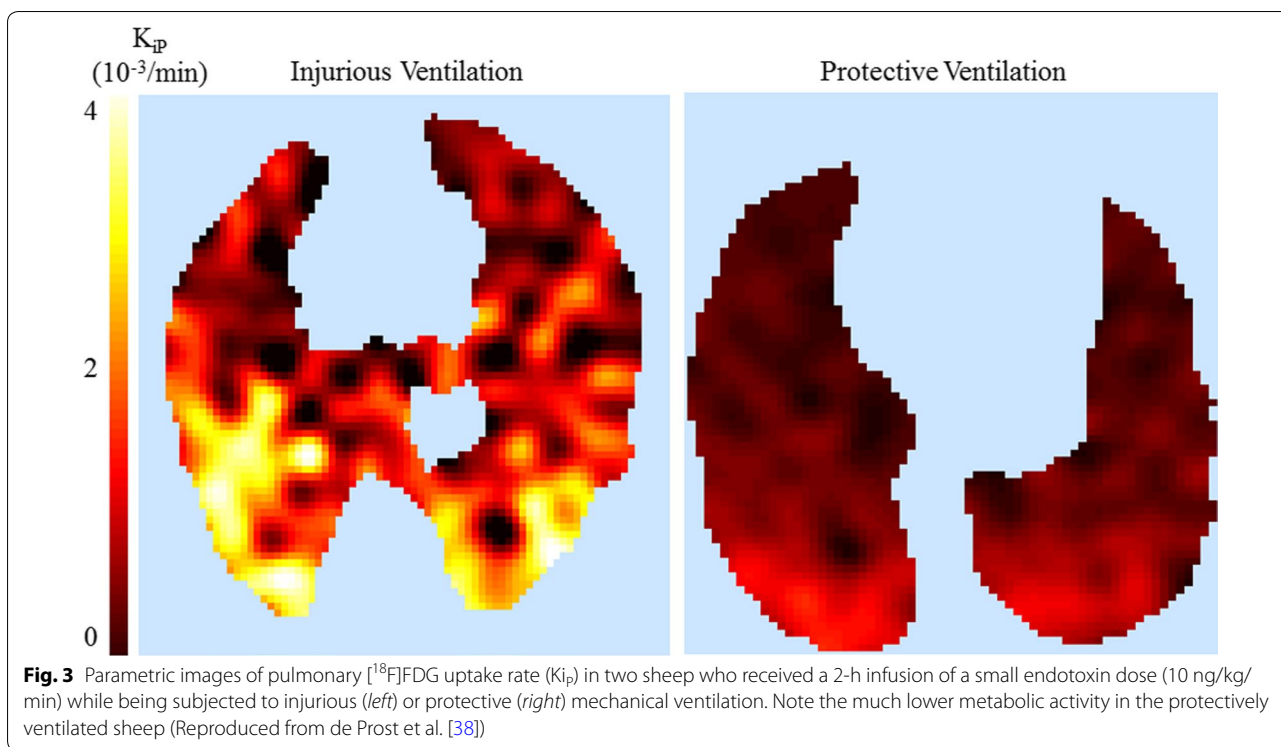


Fig. 2 Distribution of ^{18}F FDG uptake (K_i) as a function of regional lung density (CT_D) in ten patients with ARDS (dotted lines) compared with that of four controls (solid line mean, bars standard deviation). In some patients K_i increased linearly with CT_D (open symbols); this was not the case for other patients (filled symbols). Note that, in all patients, the metabolic rate was systematically increased across the entire spectrum of normal lung attenuation (Reproduced from Bellani et al. [84])

(Fig. 2). This observation suggests that metabolic activation of inflammatory cells in the normally aerated lung may be due, at least in part, to the effect of mechanical ventilation, an effect exerted predominantly on the non-consolidated lung. Consistent with this hypothesis is the finding that ^{18}F FDG uptake of the normally aerated compartment is directly proportional to its regional tidal volume normalized by end-expiratory lung volume and increases sharply for plateau airway pressures higher than 27 cmH_2O [25], again indicating that this portion of the ARDS lung may be inflamed by mechanical ventilation.

Subsequent experimental studies [36] have indeed shown a direct linear relationship between regional lung volumetric strain, measured by respiratory gating of inhaled $^{13}\text{N}_2$ PET scans, and rate of phosphorylation of ^{18}F FDG, which has been shown to correlate with expression of inflammatory cytokines IL-1 β , IL-8, and IL-10 in experimental acute lung injury [37]. Moreover, endotoxemia, an experimental surrogate for sepsis that often accompanies ARDS, increases the susceptibility of the lung to a given strain, pointing to a deleterious synergism between such an insult and VILI. This synergism implies that the benefits of protective mechanical ventilation will be enhanced in the presence of endotoxemia even when it is mild and insufficient to generate pulmonary edema per se [38] (Fig. 3).

While the role of large tidal volume and end-inspiratory lung overdistension in the pathogenesis of VILI is well established, that of end-expiratory alveolar recruitment-derecruitment is less definitive, at least in vivo [25, 39, 40].



Future directions

While routine PET scanning of ARDS patients is not feasible, PET could be useful in selected cases. Recent experimental [41] and clinical [42] studies suggest that a diffuse increase of $[^{18}\text{F}]\text{FDG}$ pulmonary uptake precedes the development of clinically manifest ARDS. Consequently, PET with $[^{18}\text{F}]\text{FDG}$ could suggest early therapy in cases at high risk of developing ARDS. Another potential clinical application of PET with $[^{18}\text{F}]\text{FDG}$ is to monitor the efficacy of anti-inflammatory treatment [43].

Recently, new PET tracers and techniques have been developed to image other aspects of lung inflammation, such as inducible nitric oxide synthase expression [44], as well as pulmonary gene expression [45]. The current availability of combined PET-CT and, in the near future, PET-MR scanners [46] makes multimodality imaging a valuable tool to further our understanding of ARDS.

Ultrasound in ARDS

Lung ultrasound basics

The use of ultrasound as a lung diagnostic tool dates back to the 1960s but only recently its use spread in the critical care setting. Gas-filled anatomical structures do not transmit ultrasound waves, normally preventing the lung visualization. Real images therefore appear only in case of pleural effusion and lung consolidation. However, air generates artifacts and lung ultrasound takes advantage of specific artifact features. Normally aerated or

hyperinflated lung (or pneumothorax) generates horizontal artifacts parallel to the pleural line (“A lines”, Fig. 4 and video 1) whereas partial loss of aeration generates longitudinal laser-like artifacts (“B lines”, Fig. 4; video 2). The number of B lines and their spatial distribution (regularly or irregularly spaced, coalescent) can be used to assess the severity of the loss of aeration and suggest diagnosis. Lung ultrasound is dynamic: lung sliding, i.e., the mutual gliding of visceral and parietal pleura synchronous with breathing, is a sign of lung ventilation. Lung sliding should not be confused with the so-called lung pulse, a sort of “heart noise” that is a short and high rate pleural movement synchronous with heartbeat (video 2). The combination of static and dynamic information allows independent evaluation of regional lung aeration and ventilation. Lung semiotics are outlined in international recommendations [47] and textbooks [48].

Lung ultrasound for diagnosis of ARDS

Lung ultrasound findings may facilitate the diagnosis in acute respiratory failure (ARF) patients [49]. In particular, ARDS presents multiple B lines, typically with a non-homogeneous non-gravity-dependent distribution, pleural thickening, subpleural consolidations, decreased or abolished lung sliding, spared areas especially in anterior regions and in the early stage of the disease and lung consolidation in dependent lung regions (Fig. 4; videos 2, 3). The bedside lung ultrasound in emergency

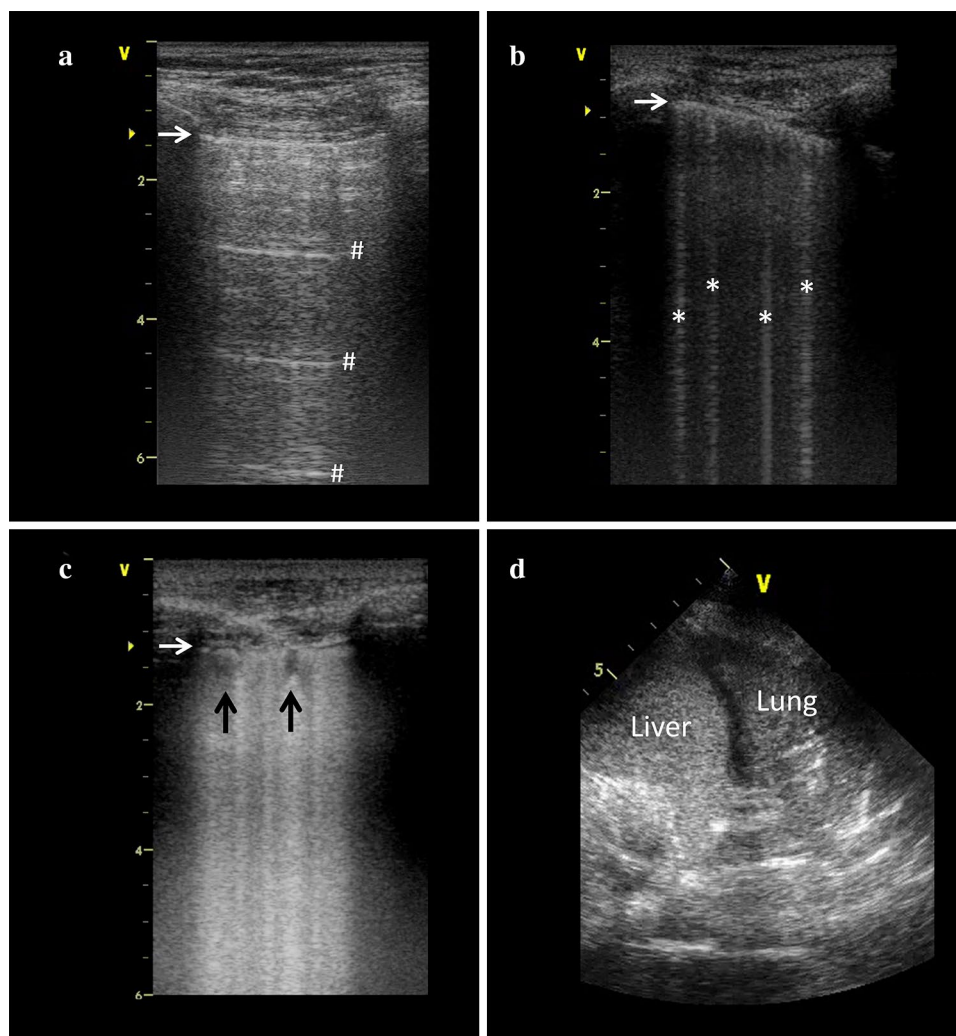


Fig. 4 Ultrasound patterns at different degrees of lung aeration. **a** Normal lung ultrasound pattern (score = 0). **b** Well-spaced B lines (moderate loss of aeration; score = 1). **c** Coalescent B lines (severe loss of aeration; score = 2). **d** Consolidated lung (complete loss of aeration; score = 3). Horizontal arrows refer to pleural line between two rib shadows. In **a** and **b**, symbols mark A lines (asterisk) and B lines (hash). In **c**, black arrows mark two small—hypoechoic—subpleural consolidations. In **d**, multiple linear and arborescent—hyperechoic—air bronchograms are clearly detectable within the lung consolidation. To compute the lung ultrasound score, six standard areas are considered in each hemithorax: anterior, lateral, and posterior regions, each divided into upper and lower fields. Lung ultrasound score corresponds to the sum of each area's score, ranging therefore from 0 (all areas normally aerated) to 36 (all regions consolidated)

(BLUE) protocol is a decision-tree proposed to translate these findings into clinical practice [50]. It is based on the assessment of (1) presence of A lines or B lines, (2) presence or absence of lung sliding, (3) presence or absence of lung consolidation and/or pleural effusion at lung ultrasound evaluation of anterior (items 1 and 2) and posterolateral (item 3) regions. These items are conveniently grouped in order to define lung ultrasound profiles associated with different causes of ARF (Table 1). Pneumonia and ARDS were associated with the B' profile (anterior B lines without lung sliding), the A/B profile (predominant B lines on one side and predominant A lines on the

other side), the C profile (anterior consolidations), and the A[V]-PLAPS profile (anterior A lines and posterolateral alveolar consolidation/pleural effusion with no deep vein thrombosis) [50].

One of the authors of the present review (D.L.) applied the BLUE protocol in 100 consecutive patients with early ARDS: anterior lung sliding was extensively or regionally abolished in 45 %, PLAPS were almost always present and a profile consistent with ARDS was allocated to 74 % of patients (data not published). Lung ultrasound can be a valid alternative to chest radiography or CT scan in most occasions. Recently a modified Berlin definition of

Table 1 Bedside lung ultrasound in emergency (BLUE) profiles (adapted from [50])

Profiles of BLUE protocol	Diagnosis ^b	Sensitivity (%)	Specificity	Main differential diagnoses
A profile: anterior bilateral lung siding with A lines (1) with no DVT and no PLAPS: the nude profile	Exacerbated COPD or severe acute asthma	89	97	Pulmonary embolism
A profile (2) with DVT	Pulmonary embolism	81	99	Incidental DVT
B profile: anterior bilateral and symmetrical lung sliding with diffuse anterior lung rockets	Acute hemodynamic pulmonary edema	97	95	Some ARDS Chronic interstitial syndromes
A' profile: A profile without lung sliding	Pneumothorax	88	100	If lung point ^a : no alternative diagnosis. Without: pleural symphysis
C profile: anterior lung consolidation (regardless size and number)	Pneumonia/ARDS	21.5	99	The few cases of anterior lung infarction
B' profile: B profile with abolished lung sliding)	Pneumonia/ARDS	11	100	None
A/B profile: one lung with half A profile, the other lung with half B profile	Pneumonia/ARDS	14.5	100	None
A profile with no DVT and with PLAPS: the A-V-PLAPS profile	Pneumonia/ARDS	42	96	Pulmonary embolism

DVT deep venous thrombosis, PLAPS posterolateral alveolar and/or pleural syndrome

^a The physical location where the lung adheres to the parietal pleura in a patient with a pneumothorax and where a location with abolished lung sliding transitions into an area of sliding, which represents the physical limit of pneumothorax as mapped on the chest wall

^b Diagnoses found in 97% of adult patients seen in the ER and admitted to the ICU of a parisian, university-affiliated hospital. The 3% remaining causes are multiple, yet each of them can benefit from one of these 8 profiles

ARDS based on lung ultrasound-detected bilateral lung opacities was used to assess incidence and outcomes of ARDS patients in resource-constrained settings [51]. Lung ultrasound also helps in differentiating patients with “white” lungs at standard chest x-ray: it easily detects and/or excludes conditions such as pleural effusions or cardiogenic pulmonary edema [47–50, 52, 53]. Lung ultrasound can predict ARDS in specific settings: ultrasound quantification of lung contusion identifies trauma patients at risk of developing ARDS [54].

Lung ultrasound-guided management of ARDS patients

In ARDS patients lung ultrasound evaluation of overall and regional lung aeration may help the assessment of illness severity, guide therapeutic interventions, and monitor the patient’s response [55]. A human model of controlled lung de-aeration identified four patterns of progressive loss of aeration [56]. A lines correspond to normally aerated or hyperinflated lung, well-spaced B lines to moderate loss of aeration, coalescent B lines to severe loss of aeration, and tissue-like pattern to complete loss of aeration (Fig. 4). A simple qualitative lung ultrasound evaluation can predict response to recruitment maneuvers: ARDS patients with diffuse loss of aeration had higher level of PEEP-induced lung recruitment if compared to patients with focal loss of aeration [17].

A lung ultrasound-based aeration score (see Fig. 4 for details) can also be obtained at the bedside, allowing

semiquantification of lung aeration [55, 57]. Lung ultrasound score showed good correlation with findings of both quantitative CT and transpulmonary thermodilution EVLW measurements [58, 59]. Moreover, in the early phase of ARDS associated with septic shock, lung ultrasound score revealed the lung aeration impairment resulting from fluid loading: thus, it was proposed as a “safeguard” against excessive fluid resuscitation [60]. The lung ultrasound re-aeration score accurately assessed the therapeutic result after 7 days of antimicrobial therapy in patients with ventilator-associated pneumonia (VAP) [61] and allowed the detection of PEEP-induced lung recruitment in ARDS patients [17]. This suggests that any intervention aimed at aeration improvement (recruitment maneuvers, prone position, bronchoscopy; see videos 4A, B) could be monitored by lung ultrasound [55, 57]. Lung ultrasound also helps early detection and appropriate treatment of lung complications in ventilated patients. Lung ultrasound has a very high diagnostic accuracy for both pneumothorax (video 1) and pleural effusions and improves safety and efficacy of thoracentesis [52]. The ventilator-associated pneumonia (VAP) ultrasound score based on specific lung ultrasound signs (Fig. 4, videos 3, 5) helps early diagnosis of VAP in ICU patients [62]. Finally, ultrasound-based assessment of heart–lung interaction can guide therapeutic interventions in ARDS patients developing acute cor pulmonale and/or shunting across a patent foramen ovale [63, 64].

Lung ultrasound technique has some limitations. Lung ultrasound cannot detect lung overinflation,

even if abolished lung sliding in non-dependent lung regions may suggest it. Subcutaneous emphysema and the presence of large thoracic dressings may preclude propagation of ultrasound beams to the lung surface. Moreover, in the case of severe chest trauma or burns the lung ultrasound examination may be limited by the patient's pain and discomfort. Care should be taken in order to avoid the transmission of infective agents by the ultrasound probe. Training is required in order to correctly perform lung ultrasound examination and interpret the findings. Finally, even if lung ultrasound is a highly repeatable technique, it is not a continuous monitoring tool.

Electrical impedance tomography (EIT) in ARDS

Electrical impedance measures the opposition that a circuit presents to alternating electric currents and can be used in many fields, from geology to medical imaging [65]. Its measurements require the application around the volume of interest of multiple pairs of electrodes transmitting a low-intensity alternating current: cross-sectional voltages are measured on the boundaries and the impedance of the region is reconstructed to obtain two- or three-dimensional images. Typically chest EIT is obtained by placing an electrode belt around the thorax, between the third and the sixth intercostal space [66]. The resulting image represents the impedance changes occurring in a cross section of the thorax, typically as thick as 5–10 cm [67].

Pulmonary ventilation EIT signal

EIT has been extensively studied to monitor regional lung ventilation [65]. Lungs are a good target for EIT because lung impedance is closely related to the degree of parenchymal inflation [67]. EIT systems generate images which do not display anatomical structures, but lung regions that present cyclic variations in lung impedance. Not ventilated (and not perfused) regions remain silent (not seen) in the EIT images. Many studies confirmed EIT's good precision to estimate the distribution of gas volume during spontaneous breathing [67, 68] or during mechanical ventilation and following changes in the ventilatory settings [69, 70]. The resolution of the image is typically one-fifth of the thoracic diameter. More recent studies validated EIT for the measurement of end-expiratory lung volume (EELV) versus nitrogen washout test and plethysmography [67, 68] or for the measurement of regional distribution of lung volume versus CT scan [71, 72], single-photon emission computed tomography (SPECT) [73], and PET [74]. EIT is widely considered a radiation-free, noninvasive continuous monitor of lung volume during ventilation [75], and possibly a guide to optimal ventilatory care [69, 70] (Fig. 5).

Pulmonary perfusion EIT signal

Impedance properties are sensitive to the difference between blood and air: therefore, EIT has also been studied to assess the regional distribution of perfusion and its relationship with ventilation. The pulmonary perfusion has been studied by EIT using two approaches measuring impedance changes, either caused by pulsatility of blood flow through the lung or caused by the first pass of a hypertonic sodium chloride bolus injected in the right atrium [76]. The first-pass contrast method was validated against a reference perfusion SCAN (SPECT and dynamic CT). This test validated EIT to provide reliable bedside information on lung perfusion [76]. Ongoing studies in patients with pulmonary embolism are under way. The lung pulsatility method so far has been shown to provide qualitative information about lung perfusion, e.g., following the activation of hypoxic pulmonary vasoconstriction, or in chronic patients who develop emphysema or pulmonary hypertension [66]. Conversely, the administration of epoprostenol in patients with pulmonary hypertension caused a marked and acute increase in EIT pulsatility [77].

EIT applications in ARDS patients

EIT detects differences in regional ventilation to monitor (a) lung heterogeneities caused by disease, (b) the effects of ventilatory maneuvers (e.g., assessment of lung recruitability), and (c) to measure the physiological effects of PEEP and tidal volume [69, 70, 72, 73, 78].

In ARDS interstitial edema enhances the gravity effects on the lung. Typically, EIT monitoring during edema formation reveals a decrease in lung aeration in dorsal regions, associated with a decrease in regional ventilation. In association with such changes, EIT typically discloses compensatory increases in regional ventilation of ventral regions [70–72, 78, 79]. This shift in ventilation distribution is so consistent and enhanced by lung weight that, recently, Trepte et al. [80] were able to quantify the EVLW during experimental acute lung injury by measuring this shift in EIT ventilation during ventilation in different body positions.

In spontaneously breathing normal subjects ventilation is higher in the dorsal lung. This is caused by the greater apposition of the dorsal diaphragm, as well as by gravity, bringing the dependent lung to a better part of P - V curve, with better regional compliance [79]. In the presence of increased lung weight, or during the loss of muscle tone, however, airway closure and increased pleural pressures in dependent zones tend to reverse this pattern, and ventilation predominates in the non-dependent lung. This abnormal shift is detectable by EIT, as are the changes in the patency of dorsal lung units due to the effects of tidal volume [69], PEEP [75],

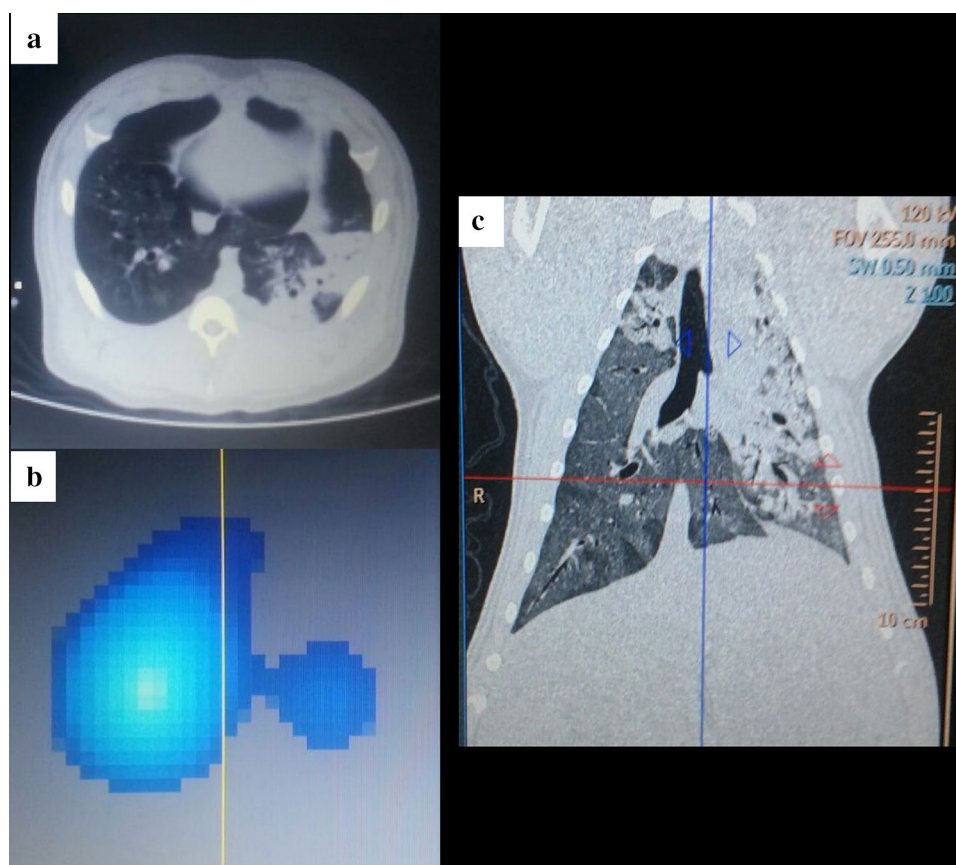


Fig. 5 EIT represents a very thick slice of the lung. Note that cross-sectional axial CT image (0.5 cm) **(a)** does not show much of an impairment of left lung, whereas the EIT shows a big deficit in the left lung **(b)**. Then, when looking at the coronal view **(c)**, one can understand that the EIT was disclosing the great impairment of left lung in regions well above the cross-sectional plane. This animal had ARDS plus pneumonia

and recruitment maneuvers (RM) [70]. Maneuvers that enhance dorsal ventilation (sighs, recruiting maneuvers, or higher PEEP in association with lower V_T) consistently improve oxygenation [69], dorsal ventilation [70], and lung protection in experimental studies [67, 80]. In contrast, high pressure support levels or tidal volumes are associated with increased ventral ventilation and signals of non-dependent lung overdistension. Moreover, EIT-derived regional compliance (calculated as tidal changes in pixel impedance divided by airway driving pressures [71]), when measured serially during PEEP titration, has been used to calculate the percentage of collapsed lung units estimated by CT [79] or to distinguish between potentially recruitable or non-recruitable lung zones [71]. During incremental and decremental PEEP trials, new indexes like EIT-derived “intratidal gas distribution” and EIT-derived “hyperdistension” have been calculated and shown to be promising indexes to detect excessive lung strain [81, 82]. Finally, ARDS patients can be clearly distinguished from patients with

healthy lungs by calculating EIT-derived regional time constants [70, 71]. Not only time constants but also other dynamic intratidal indexes of lung inflation are promising in detecting pathological conditions like tidal recruitment and pendelluft, the latter typically caused by excessive patient efforts. When pendelluft occurs, the possibility of overstretch of the dependent lung is strongly suggested by EIT, even in patients submitted to low tidal volume ventilation [82].

EIT limitations and future developments

Current research is aimed at enlarging EIT’s field of application by improving image reconstruction algorithms, creating dedicated algorithms for specific clinical applications, improving its communication with ventilators, correcting artifacts caused by changes in thoracic shape, and providing three-dimensional absolute/relative images with better resolution. The study of lung pulsatility will soon require faster EIT imaging systems and advanced temporal filtering processes [67].

Conclusion

Imaging in ARDS is likely the most relevant procedure that allowed a better understanding of the syndrome, leading to a quantitative definition of concepts such as normal, hyper-, or non-inflation, recruitability, and lung inhomogeneity. To date it still represents the best approach to characterize ARDS in the individual patients. A brief note should be written on the use of other techniques such as magnetic resonance imaging (MRI) in lung image assessments; in fact, although its use has been limited mainly to research, MRI when combined with regional measures of perfusion provides a new method to measure the regional distribution of ventilation/perfusion [83]. Finally, if, in the near future, CT scan technology allows acquisition at the bedside at low x-ray exposure, its use should greatly expand, allowing, we believe, a more rational approach to ARDS treatment.

Electronic supplementary material

The online version of this article (doi:[10.1007/s00134-016-4328-1](https://doi.org/10.1007/s00134-016-4328-1)) contains supplementary material, which is available to authorized users.

Author details

¹ Dipartimento di Anestesia, Rianimazione ed Emergenza Urgenza, Fondazione IRCCS Cà Granda-Ospedale Maggiore Policlinico, Via Francesco Sforza 35, 20122 Milan, Italy. ² Dipartimento di Fisiopatologia Medico-Chirurgica e dei Trapianti, Università degli Studi di Milano, Milan, Italy. ³ Department of Anesthesiology, Washington University and General Anesthesiology, Barnes Jewish Hospital, St. Louis, USA. ⁴ Medical ICU, Hospital Ambroise-Paré, Paris-West University, Nanterre, France. ⁵ Anesthesia and Intensive Care, Emergency Department, Fondazione IRCCS Policlinico S. Matteo, Pavia, Italy. ⁶ Anesthesia, Intensive Care and Pain Therapy, Department of Clinical, Surgical, Diagnostic and Pediatric Sciences, University of Pavia, Pavia, Italy. ⁷ Respiratory Intensive Care Unit, University of Sao Paulo School of Medicine, University of Sao Paulo, Sao Paulo, Brazil. ⁸ Department of Anesthesia and Intensive Care, University of Foggia, Foggia, Italy. ⁹ Department of Anesthesiology, Emergency and Intensive Care Medicine, Georg-August University of Göttingen, Göttingen, Germany.

Acknowledgments

The authors thank Dr. Eleonora Carlesso for her support in the preparation and revision of the manuscript.

Compliance with ethical standards

Conflicts of interest

None.

Received: 24 February 2016 Accepted: 11 March 2016

Published online: 31 March 2016

References

- Bellani G, Laffey JG, Pham T et al (2016) Epidemiology, patterns of care, and mortality for patients with acute respiratory distress syndrome in intensive care units in 50 countries. *JAMA* 315:788–800. doi:[10.1001/jama.2016.0291](https://doi.org/10.1001/jama.2016.0291)
- Rommelsheim K, Lackner K, Westhofen P et al (1983) Respiratory distress syndrome of the adult in the computer tomograph. *Anästhesiologie Intensivther Notfallmedizin* 18:59–64
- Maunder RJ, Shuman WP, McHugh JW et al (1986) Preservation of normal lung regions in the adult respiratory distress syndrome. Analysis by computed tomography. *JAMA* 255:2463–2465
- Gattinoni L, Mascheroni D, Torresin A et al (1986) Morphological response to positive end expiratory pressure in acute respiratory failure. Computerized tomography study. *Intensive Care Med* 12:137–142
- Gattinoni L, Pesenti A, Avalli L et al (1987) Pressure–volume curve of total respiratory system in acute respiratory failure. Computed tomographic scan study. *Am Rev Respir Dis* 136:730–736. doi:[10.1164/ajrccm/136.3.730](https://doi.org/10.1164/ajrccm/136.3.730)
- Malbouisson LM, Muller JC, Constantin JM et al (2001) Computed tomography assessment of positive end-expiratory pressure-induced alveolar recruitment in patients with acute respiratory distress syndrome. *Am J Respir Crit Care Med* 163:1444–1450
- Reske AW, Reske AP, Gast HA et al (2010) Extrapolation from ten sections can make CT-based quantification of lung aeration more practicable. *Intensive Care Med* 36:1836–1844. doi:[10.1007/s00134-010-2014-2](https://doi.org/10.1007/s00134-010-2014-2)
- Ashbaugh DG, Bigelow DB, Petty TL, Levine BE (1967) Acute respiratory distress in adults. *Lancet* 2:319–323
- Gattinoni L, Marini JJ, Pesenti A et al (2016) The “baby lung” became an adult. *Intensive Care Med*. doi:[10.1007/s00134-015-4200-8](https://doi.org/10.1007/s00134-015-4200-8)
- Terragni PP, Rosboch G, Tealdi A et al (2007) Tidal hyperinflation during low tidal volume ventilation in acute respiratory distress syndrome. *Am J Respir Crit Care Med* 175:160–166
- Pelosi P, D’Andrea L, Vitale G et al (1994) Vertical gradient of regional lung inflation in adult respiratory distress syndrome. *Am J Respir Crit Care Med* 149:8–13. doi:[10.1164/ajrccm.149.1.8111603](https://doi.org/10.1164/ajrccm.149.1.8111603)
- Gattinoni L, D’Andrea L, Pelosi P et al (1993) Regional effects and mechanism of positive end-expiratory pressure in early adult respiratory distress syndrome. *JAMA* 269:2122–2127
- Gattinoni L, Caironi P, Cressoni M et al (2006) Lung recruitment in patients with the acute respiratory distress syndrome. *N Engl J Med* 354:1775–1786. doi:[10.1056/NEJMoa052052](https://doi.org/10.1056/NEJMoa052052)
- Briel M, Meade M, Mercat A et al (2010) Higher vs lower positive end-expiratory pressure in patients with acute lung injury and acute respiratory distress syndrome: systematic review and meta-analysis. *JAMA* 303:865–873
- Falke KJ, Pontoppidan H, Kumar A et al (1972) Ventilation with end-expiratory pressure in acute lung disease. *J Clin Invest* 51:2315–2323
- Gattinoni L, Pelosi P, Suter PM et al (1998) Acute respiratory distress syndrome caused by pulmonary and extrapulmonary disease. Different syndromes? *Am J Respir Crit Care Med* 158:3–11. doi:[10.1164/ajrccm.158.1.9708031](https://doi.org/10.1164/ajrccm.158.1.9708031)
- Bouhemad B, Brisson H, Le Guen M et al (2011) Bedside ultrasound assessment of positive end-expiratory pressure-induced lung recruitment. *Am J Respir Crit Care Med* 183:341–347
- Kunst PW, Vazquez de Anda G, Böhm SH et al (2000) Monitoring of recruitment and derecruitment by electrical impedance tomography in a model of acute lung injury. *Crit Care Med* 28:3891–3895
- Chiumello D, Marino A, Brioni M et al (2015) Lung recruitment assessed by respiratory mechanics and by CT scan: what is the relationship? *Am J Respir Crit Care Med*. doi:[10.1164/rccm.201507-1413OC](https://doi.org/10.1164/rccm.201507-1413OC)
- Chiumello D, Carlesso E, Cadringer P et al (2008) Lung stress and strain during mechanical ventilation for acute respiratory distress syndrome. *Am J Respir Crit Care Med* 178:346–355
- Cressoni M, Cadringer P, Chiurazzi C et al (2014) Lung inhomogeneity in patients with acute respiratory distress syndrome. *Am J Respir Crit Care Med* 189:149–158. doi:[10.1164/rccm.201308-1567OC](https://doi.org/10.1164/rccm.201308-1567OC)
- Vecchi V, Langer T, Bellomi M et al (2013) Low-dose CT for quantitative analysis in acute respiratory distress syndrome. *Crit Care Med* 41:R183. doi:[10.1186/cc12866](https://doi.org/10.1186/cc12866)
- Caironi P, Carlesso E, Cressoni M et al (2015) Lung recruitability is better estimated according to the Berlin definition of acute respiratory distress syndrome at standard 5 cmH₂O rather than higher positive end-expiratory pressure: a retrospective cohort study. *Crit Care Med* 43:781–790. doi:[10.1097/CCM.0000000000000770](https://doi.org/10.1097/CCM.0000000000000770)
- Chiumello D, Marino A, Cressoni M et al (2013) Pleural effusion in patients with acute lung injury: a CT scan study. *Crit Care Med* 41:935–944
- Bellani G, Guerra L, Musch G et al (2011) Lung regional metabolic activity and gas volume changes induced by tidal ventilation in patients with acute lung injury. *Am J Respir Crit Care Med* 183:1193–1199. doi:[10.1164/rccm.201008-1318OC](https://doi.org/10.1164/rccm.201008-1318OC)
- Schuster DP (1998) The evaluation of lung function with PET. *Semin Nucl Med* 28:341–351

27. Sandiford P, Province MA, Schuster DP (1995) Distribution of regional density and vascular permeability in the adult respiratory distress syndrome. *Am J Respir Crit Care Med* 151:737–742. doi:[10.1164/ajrccm/151.3_Pt_1.737](https://doi.org/10.1164/ajrccm/151.3_Pt_1.737)
28. Schuster DP, Anderson C, Kozlowski J, Lange N (2002) Regional pulmonary perfusion in patients with acute pulmonary edema. *J Nucl Med* 43:863–870
29. Musch G, Harris RS, Vidal Melo MF et al (2004) Mechanism by which a sustained inflation can worsen oxygenation in acute lung injury. *Anesthesiology* 100:323–330
30. Musch G, Bellani G, Vidal Melo MF et al (2008) Relation between shunt, aeration, and perfusion in experimental acute lung injury. *Am J Respir Crit Care Med* 177:292–300. doi:[10.1164/rccm.200703-484OC](https://doi.org/10.1164/rccm.200703-484OC)
31. Richter T, Bergmann R, Musch G et al (2015) Reduced pulmonary blood flow in regions of injury 2 hours after acid aspiration in rats. *BMC Anesthesiol* 15:36. doi:[10.1186/s12871-015-0013-0](https://doi.org/10.1186/s12871-015-0013-0)
32. Jones HA, Clark RJ, Rhodes CG et al (1994) In vivo measurement of neutrophil activity in experimental lung inflammation. *Am J Respir Crit Care Med* 149:1635–1639. doi:[10.1164/ajrccm.149.6.7516252](https://doi.org/10.1164/ajrccm.149.6.7516252)
33. Chen DL, Schuster DP (2004) Positron emission tomography with [¹⁸F] fluorodeoxyglucose to evaluate neutrophil kinetics during acute lung injury. *Am J Physiol Lung Cell Mol Physiol* 286:L834–L840. doi:[10.1152/ajplung.00339.2003](https://doi.org/10.1152/ajplung.00339.2003)
34. Musch G, Venegas JG, Bellani G et al (2007) Regional gas exchange and cellular metabolic activity in ventilator-induced lung injury. *Anesthesiology* 106:723–735. doi:[10.1097/01.anes.0000264748.86145.ac](https://doi.org/10.1097/01.anes.0000264748.86145.ac)
35. Jacene HA, Cohade C, Wahl RL (2004) F-18 FDG PET/CT in acute respiratory distress syndrome: a case report. *Clin Nucl Med* 29:786–788
36. Wellman TJ, Winkler T, Costa ELV et al (2014) Effect of local tidal lung strain on inflammation in normal and lipopolysaccharide-exposed sheep. *Crit Care Med* 42:e491–e500. doi:[10.1097/CCM.0000000000000346](https://doi.org/10.1097/CCM.0000000000000346)
37. de Prost N, Feng Y, Wellman T et al (2014) 18F-FDG kinetics parameters depend on the mechanism of injury in early experimental acute respiratory distress syndrome. *J Nucl Med* 55:1871–1877. doi:[10.2967/jnumed.114.140962](https://doi.org/10.2967/jnumed.114.140962)
38. de Prost N, Costa EL, Wellman T et al (2013) Effects of ventilation strategy on distribution of lung inflammatory cell activity. *Crit Care* 17:R175. doi:[10.1186/cc12854](https://doi.org/10.1186/cc12854)
39. Cressoni M, Chiumello D, Chiurazzi C et al (2015) Lung inhomogeneities, inflation and [¹⁸F]-fluoro-2-deoxy-D-glucose uptake rate in acute respiratory distress syndrome. *Eur Respir J*. doi:[10.1183/13993003.00885-2015](https://doi.org/10.1183/13993003.00885-2015)
40. Borges JB, Costa ELV, Bergquist M et al (2015) Lung inflammation persists after 27 hours of protective Acute Respiratory Distress Syndrome Network strategy and is concentrated in the nondependent lung. *Crit Care Med* 43:e123–e132. doi:[10.1097/CCM.0000000000000926](https://doi.org/10.1097/CCM.0000000000000926)
41. Musch G, Winkler T, Harris RS et al (2014) Lung [(18)F]fluorodeoxyglucose uptake and ventilation-perfusion mismatch in the early stage of experimental acute smoke inhalation. *Anesthesiology* 120:683–693. doi:[10.1097/01.anes.0000435742.04859.e8](https://doi.org/10.1097/01.anes.0000435742.04859.e8)
42. Rodrigues RS, Miller PR, Bozza FA et al (2008) FDG-PET in patients at risk for acute respiratory distress syndrome: a preliminary report. *Intensive Care Med* 34:2273–2278. doi:[10.1007/s00134-008-1220-7](https://doi.org/10.1007/s00134-008-1220-7)
43. Chen DL, Bedient TJ, Kozlowski J et al (2009) [¹⁸F]fluorodeoxyglucose positron emission tomography for lung antiinflammatory response evaluation. *Am J Respir Crit Care Med* 180:533–539. doi:[10.1164/rccm.200904-0501OC](https://doi.org/10.1164/rccm.200904-0501OC)
44. Huang HJ, Isakow W, Byers DE et al (2015) Imaging pulmonary inducible nitric oxide synthase expression with PET. *J Nucl Med* 56:76–81. doi:[10.2967/jnumed.114.146381](https://doi.org/10.2967/jnumed.114.146381)
45. Richard JC, Brochard L, Vandelet P et al (2003) Respective effects of end-expiratory and end-inspiratory pressures on alveolar recruitment in acute lung injury. *Crit Care Med* 31:89–92
46. Cereda M, Emami K, Xin Y et al (2013) Imaging the interaction of atelectasis and overdistension in surfactant-depleted lungs. *Crit Care Med* 41:527–535. doi:[10.1097/CCM.0b013e31826ab1f2](https://doi.org/10.1097/CCM.0b013e31826ab1f2)
47. Volpicelli G, Elbarbary M, Blaivas M et al (2012) International evidence-based recommendations for point-of-care lung ultrasound. *Intensive Care Med* 38:577–591. doi:[10.1007/s00134-012-2513-4](https://doi.org/10.1007/s00134-012-2513-4)
48. Lichtenstein D (2010) Whole body ultrasonography in the critically ill. Springer-Verlag, Heidelberg
49. Copetti R, Soldati G, Copetti P (2008) Chest sonography: a useful tool to differentiate acute cardiogenic pulmonary edema from acute respiratory distress syndrome. *Cardiovasc Ultrasound* 6:16. doi:[10.1186/1476-7120-6-16](https://doi.org/10.1186/1476-7120-6-16)
50. Lichtenstein DA, Mezière GA (2008) Relevance of lung ultrasound in the diagnosis of acute respiratory failure: the BLUE protocol. *Chest* 134:117–125. doi:[10.1378/chest.07-2800](https://doi.org/10.1378/chest.07-2800)
51. Riviello ED, Kiviri W, Twagirumugabe T et al (2016) Hospital incidence and outcomes of the acute respiratory distress syndrome using the Kigali modification of the Berlin definition. *Am J Respir Crit Care Med* 193:52–59. doi:[10.1164/rccm.201503-0584OC](https://doi.org/10.1164/rccm.201503-0584OC)
52. Lichtenstein D, Hulot JS, Rabiller A et al (1999) Feasibility and safety of ultrasound-aided thoracentesis in mechanically ventilated patients. *Intensive Care Med* 25:955–958
53. Lichtenstein DA, Mezière GA, Lagoueyte J-F et al (2009) A-lines and B-lines: lung ultrasound as a bedside tool for predicting pulmonary artery occlusion pressure in the critically ill. *Chest* 136:1014–1020. doi:[10.1378/chest.09-0001](https://doi.org/10.1378/chest.09-0001)
54. Leblanc D, Bouvet C, Degiovanni F et al (2014) Early lung ultrasonography predicts the occurrence of acute respiratory distress syndrome in blunt trauma patients. *Intensive Care Med* 40:1468–1474. doi:[10.1007/s00134-014-3382-9](https://doi.org/10.1007/s00134-014-3382-9)
55. Bouhemad B, Mongodi S, Via G, Rouquette I (2015) Ultrasound for “lung monitoring” of ventilated patients. *Anesthesiology* 122:437–447. doi:[10.1097/ALN.0000000000000558](https://doi.org/10.1097/ALN.0000000000000558)
56. Via G, Lichtenstein D, Mojoli F et al (2010) Whole lung lavage: a unique model for ultrasound assessment of lung aeration changes. *Intensive Care Med* 36:999–1007. doi:[10.1007/s00134-010-1834-4](https://doi.org/10.1007/s00134-010-1834-4)
57. Via G, Storti E, Gulati G et al (2012) Lung ultrasound in the ICU: from diagnostic instrument to respiratory monitoring tool. *Minerva Anestesiol* 78:1282–1296
58. Mongodi S, Algieri I, Mojoli F et al (2014) CT scan and ultrasound comparative assessment of lung aeration in ARDS. *Intensive Care Med* 40:S445
59. Zhao Z, Jiang L, Xi X et al (2015) Prognostic value of extravascular lung water assessed with lung ultrasound score by chest sonography in patients with acute respiratory distress syndrome. *BMC Pulm Med* 15:98. doi:[10.1186/s12890-015-0091-2](https://doi.org/10.1186/s12890-015-0091-2)
60. Caltabelotti F, Monsel A, Arbelot C et al (2014) Early fluid loading in acute respiratory distress syndrome with septic shock deteriorates lung aeration without impairing arterial oxygenation: a lung ultrasound observational study. *Crit Care* 18:R91. doi:[10.1186/cc13859](https://doi.org/10.1186/cc13859)
61. Bouhemad B, Liu Z-H, Arbelot C et al (2010) Ultrasound assessment of antibiotic-induced pulmonary reaeration in ventilator-associated pneumonia. *Crit Care Med* 38:84–92. doi:[10.1097/CCM.0b013e3181b08cdb](https://doi.org/10.1097/CCM.0b013e3181b08cdb)
62. Mongodi S, Via G, Girard M et al (2015) Lung ultrasound for early diagnosis of ventilator-associated pneumonia. *Chest*. doi:[10.1016/j.chest.2015.12.012](https://doi.org/10.1016/j.chest.2015.12.012)
63. Mekontso Dessap A, Boissier F, Charron C et al (2015) Acute cor pulmonale during protective ventilation for acute respiratory distress syndrome: prevalence, predictors, and clinical impact. *Intensive Care Med*. doi:[10.1007/s00134-015-4141-2](https://doi.org/10.1007/s00134-015-4141-2)
64. Mekontso Dessap A, Boissier F, Leon R et al (2010) Prevalence and prognosis of shunting across patent foramen ovale during acute respiratory distress syndrome. *Crit Care Med* 38:1786–1792. doi:[10.1097/CCM.0b013e3181eaa9c8](https://doi.org/10.1097/CCM.0b013e3181eaa9c8)
65. Brown BH (2003) Electrical impedance tomography (EIT): a review. *J Med Eng Technol* 27:97–108. doi:[10.1080/0309190021000059687](https://doi.org/10.1080/0309190021000059687)
66. Roth CJ, Ehrl A, Becher T et al (2015) Correlation between alveolar ventilation and electrical properties of lung parenchyma. *Physiol Meas* 36:1211–1226. doi:[10.1088/0967-3334/36/6/1211](https://doi.org/10.1088/0967-3334/36/6/1211)
67. Adler A, Amato MB, Arnold JH et al (2012) Whither lung EIT: where are we, where do we want to go and what do we need to get there? *Physiol Meas* 33:679–694. doi:[10.1088/0967-3334/33/5/679](https://doi.org/10.1088/0967-3334/33/5/679)
68. Costa ELV, Lima RG, Amato MBP (2009) Electrical impedance tomography. *Curr Opin Crit Care* 15:18–24
69. Mauri T, Bellani G, Confalonieri A et al (2013) Topographic distribution of tidal ventilation in acute respiratory distress syndrome: effects of positive end-expiratory pressure and pressure support. *Crit Care Med* 41:1664–1673. doi:[10.1097/CCM.0b013e318287f6e7](https://doi.org/10.1097/CCM.0b013e318287f6e7)

70. Cinnella G, Grasso S, Raimondo P et al (2015) Physiological effects of the open lung approach in patients with early, mild, diffuse acute respiratory distress syndrome: an electrical impedance tomography study. *Anesthesiology* 123:1113–1121. doi:[10.1097/ALN.0000000000000862](https://doi.org/10.1097/ALN.0000000000000862)
71. Victorino JA, Borges JB, Okamoto VN et al (2004) Imbalances in regional lung ventilation: a validation study on electrical impedance tomography. *Am J Respir Crit Care Med* 169:791–800. doi:[10.1164/rccm.200301-133OC](https://doi.org/10.1164/rccm.200301-133OC)
72. Pulletz S, Kott M, Elke G et al (2012) Dynamics of regional lung aeration determined by electrical impedance tomography in patients with acute respiratory distress syndrome. *Multidiscip Respir Med* 7:44. doi:[10.1186/2049-6958-7-44](https://doi.org/10.1186/2049-6958-7-44)
73. Nguyen DT, Thiagalingam A, Bhaskaran A et al (2014) Electrical impedance tomography for assessing ventilation/perfusion mismatch for pulmonary embolism detection without interruptions in respiration. *Conf Proc IEEE Eng Med Biol Soc* 2014:6068–6071. doi:[10.1109/EMBC.2014.6945013](https://doi.org/10.1109/EMBC.2014.6945013)
74. Richard JC, Pouzot C, Gros A et al (2009) Electrical impedance tomography compared to positron emission tomography for the measurement of regional lung ventilation: an experimental study. *Crit Care* 13:R82. doi:[10.1186/cc7900](https://doi.org/10.1186/cc7900)
75. Karsten J, Heinze H, Meier T (2014) Impact of PEEP during laparoscopic surgery on early postoperative ventilation distribution visualized by electrical impedance tomography. *Minerva Anesthesiol* 80:158–166
76. Borges JB, Suarez-Sipmann F, Bohm SH et al (2012) Regional lung perfusion estimated by electrical impedance tomography in a piglet model of lung collapse. *J Appl Physiol* 112:225–236. doi:[10.1152/jappphysiol.01090.2010](https://doi.org/10.1152/jappphysiol.01090.2010)
77. Smit HJ, Vonk Noordegraaf A, Roeleveld RJ et al (2002) Epoprostenol-induced pulmonary vasodilatation in patients with pulmonary hypertension measured by electrical impedance tomography. *Physiol Meas* 23:237–243
78. Bellani G, Mauri T, Pesenti A (2012) Imaging in acute lung injury and acute respiratory distress syndrome. *Curr Opin Crit Care* 18:29–34. doi:[10.1097/MCC.0b013e32834eb47d](https://doi.org/10.1097/MCC.0b013e32834eb47d)
79. Costa ELV, Borges JB, Melo A et al (2009) Bedside estimation of recruitable alveolar collapse and hyperdistension by electrical impedance tomography. *Intensive Care Med* 35:1132–1137. doi:[10.1007/s00134-009-1447-y](https://doi.org/10.1007/s00134-009-1447-y)
80. Trepte CJC, Phillips CR, Solà J et al (2016) Electrical impedance tomography (EIT) for quantification of pulmonary edema in acute lung injury. *Crit Care* 20:18. doi:[10.1186/s13054-015-1173-5](https://doi.org/10.1186/s13054-015-1173-5)
81. Blankman P, Hasan D, Erik G, Gommers D (2014) Detection of “best” positive end-expiratory pressure derived from electrical impedance tomography parameters during a decremental positive end-expiratory pressure trial. *Crit Care* 18:R95. doi:[10.1186/cc13866](https://doi.org/10.1186/cc13866)
82. Bikker IG, Blankman P, Specht P et al (2013) Global and regional parameters to visualize the “best” PEEP during a PEEP trial in a porcine model with and without acute lung injury. *Minerva Anesthesiol* 79:983–992
83. Henderson AC, Sá RC, Theilmann RJ et al (2013) The gravitational distribution of ventilation–perfusion ratio is more uniform in prone than supine posture in the normal human lung. *J Appl Physiol* 115:313–324. doi:[10.1152/jappphysiol.01531.2012](https://doi.org/10.1152/jappphysiol.01531.2012)
84. Bellani G, Messa C, Guerra L et al (2009) Lungs of patients with acute respiratory distress syndrome show diffuse inflammation in normally aerated regions: a [18F]-fluoro-2-deoxy-D-glucose PET/CT study. *Crit Care Med* 37:2216–2222. doi:[10.1097/CCM.0b013e3181aab31f](https://doi.org/10.1097/CCM.0b013e3181aab31f)